Nanosized SnSb Alloy Pinning on Hard Non-Graphitic Carbon Spherules as Anode Materials for a Li Ion Battery

Hong Li, Qing Wang, Lihong Shi, Liquan Chen, and Xuejie Huang*

Institute of Physics, Chinese Academy of Sciences, Beijing 100080, China

Received March 7, 2001. Revised Manuscript Received August 22, 2001

Nanosized SnSb alloy particles were pinned on the surface of micrometer-sized hard carbon spherules by a coprecipitation method in glycol solution at low temperature. Thanks to the small alloy particle size, good dispersion, and tight pinning of the alloy particles on the surface of carbon, in addition to the fact that both the alloy and the carbon are active for Li storage, the composite materials as prepared show much improved electrochemical performances as anode materials for lithium ion batteries compared with alloy and carbon alone. Such a special structure effectively hinders the aggregation of nanosized alloy particles, which are the main difficulties in the application of nanoscale alloy-based anode materials for Li ion batteries.

Introduction

It has been known that many metals and alloys can store large quantity of lithium ions by the formation of alloys ($Li_{4.4}Si$, corresponding to Li storage electrochemical capacity of 4200 mA h/g; $Li_{4.4}Ge$: 1600 mA h/g; LiAl and $Li_{4.4}Sn$: 990 mA h/g; Li_3Sb: 660 mA h/g).[1,2] In contrast, the graphitic carbon materials commonly used in commercial Li ion batteries only have a Li storage capacity less than 372 mA h/g.[3,4] The main difficulties for using alloy-based materials are their dramatic volume expansion and contraction during Li insertion and extraction.[1,2] This leads to the pulverization of the electrode materials and poor cyclic performance. Fuji's amorphous tin-based composite oxides (TCO) show a high capacity of 650 mA h/g and satisfactory cyclic performance.[5] This improvement is attributed to the special microstructure in which active Sn clusters are dispersed in an oxide network at the nanometer scale.[6,7] However, a deterrent to its practical application is its lower Coulombic efficiency (Li extraction capacity/Li insertion capacity = 63% for TCO in the first cycle) caused by an unavoidable oxide reduction−replacement reaction.[6−8] Enlightened by the pioneer work on TCO, intermetallic compounds, e.g. $Sn_2Fe/SnFe_3C$ (1:4 by weight),[9] have been studied recently. In this case, active Sn atoms are dispersed into a matrix composed of inactive Fe and $SnFe_3C$ after insertion of Li ions. Its volumetric capacity is 1600 mA h/cm^3, but its gravimetric capacity is only 200 mA h/g due to the high weight ratio of inactive elements. In addition, its cyclic performance is not very satisfactory. A strategy using superfine $Sn(SnSb)_{0.14}$ (200 nm) as the anode material opened up another way to enhance the dimensional stability of the alloy because superfine alloy particles are supposed to have stronger endurance to volume variation.[10] However, the addition of unstable $Li_{2.6}Co_{0.4}N$ and inert Ni powder are still necessary to improve the structural stability and compensate low Coulombic efficiency of $Sn(SnSb)_{0.14}$ (63% at the first cycle and 93% at later cycles).[11]

Our recent studies on nanosized Sb, SnSb, and Si illustrated that these materials show very high Li storage capacity.[12−15] Furthermore, nanoscale materials have shown great potential in kinetics.[12,16] However, when the particle size of active alloy decreased to below 100 nm, micrometer-scale aggregates were commonly formed after Li insertion.[12,14,15] This leads to low efficiency and fast capacity fading so that counteracts the advantages of nanosized materials. It has been found that the electrochemical agglomeration could not be hindered completely even by mixing carbon black as dispersant with active material at a weight ratio of

* Corresponding author. E-mail: xjhuang@aphy02.iphy.ac.cn, Fax +86-10-82649050.

(1) Huggins, R. A. *J. Power Sources* **1999**, *81−82*, 13−19.
(2) Winter, M.; Besenhard, J. O.; Spahr, M.; Novak, P. *Adv. Mater.* **1998**, *10*, 725−763
(3) Sato, K.; Noguchi, M.; Demachi, A.; Oki, N.; Endo, M. *Science* **1994**, *264*, 556−558.
(4) Dahn, J. R.; Zheng, T.; Liu, Y.; Xue, J. S. *Science* **1995**, *270*, 590−593.
(5) Idota, Y.; Kubota, T.; Matsufuji, A.; Maekawa, Y.; Miyasaka, T. *Science* **1997**, *276*, 1395−1397.
(6) Courtney, I. A.; Dahn, J. R. *J. Electrochem. Soc.* **1997**, *144*, 2045−2052.
(7) Li, H.; Huang, X. J.; Chen, L. Q. *Electrochem. Solid-State Lett.* **1998**, *1*, 241−243.
(8) Liu, W. F.; Huang, X. J.; Wang, Z. X.; Li, H.; Chen, L. Q. *J. Electrochem. Soc.* **1998**, *145*, 59−62.
(9) Mao, O.; Dahn, J. R. *J. Electrochem. Soc.* **1999**, *146*, 423−427.
(10) Yang, J.; Winter, M.; Besenhard, J. O. *Solid State Ionics* **1996**, *90*, 281−287.
(11) Yang, J.; Takeda, Y.; Imanishi, N.; Yamamoto, J. *Electrochem. Soc.* **2000**, *147*, 1671−1675.
(12) Li, H.; Huang, X. J.; Chen, L. Q.; Wu, Z. G.; Liang, Y. *Electrochem. Solid-State Lett.* **1999**, *2*, 547−549.
(13) Li, H.; Zhu, G. Y.; Huang, X. J.; Chen, L. Q. *J. Mater. Chem.* **2000**, *10*, 693−696.
(14) Li, H.; Shi, L. H.; Lu, W.; Huang, X. J.; Chen, L. Q. *J. Electrochem. Soc.* **2001**, *148*, A915−A922.
(15) Li, H.; Huang, X. J.; Chen, L. Q.; Zhou, G. W.; Zhang, Z.; Yu, D. P.; Mo, Y. J.; Pei, N. *Solid State Ionics* **2000**, *135*, 181−191.
(16) Li, N. C.; Martin, C. R.; Scrosati, B. *Electrochem. Solid-State Lett.* **2000**, *3*, 316−318.

10.1021/cm010195p CCC: $22.00
Published on Web 12/27/2001

1:1.[14,15] As a result, their cyclic performance is not satisfied. On the basis of above results obtained by others and us, it is believed that improving the dimensional stability of alloy particles/clusters during Li insertion/extraction cycling is the most important factor to achieve better cyclic performance. In the present work, we propose a new strategy to solve the problems: uniformly pinning of nanosized alloy on the surface of micrometer-sized carbon particles.

Experimental Section

Materials. A kind of non-graphitic carbon material, hard carbon spherules (named HCS), was selected as the support of nanoalloy particles. The preparation and characterization of the HCS have been reported elsewhere and described briefly as follows.[17] First, aqueous sugar solution of 1.5 mol/L was filled in a stainless steel autoclave with a fill rate of 90%. After 5 h hydrothermal treatment at 190 °C, the obtained black powder was further carbonized in a tube furnace in argon atmosphere. The argon flow rate, final temperature, and heating rate of the furnace were 25 mL/min, 1000 °C, and 1 °C/min below 500 °C and 5 °C/min above 500 °C. The HCS particles show a perfect ball-like appearance. The average diameter of the particles is 6−8 μm, the BET area is 400 m^2/g, and the typical diameter of micropore within the particles is 0.4−0.8 nm according to HRTEM.[17] Therefore, the HCS is a typical nongraphized carbon. The nano-SnSb alloy/HCS composite was prepared as following. First, 22.8 g of $SbCl_3$ and 22.6 g of $SnCl_2{\cdot}2H_2O$ (AR. 99%, Beijing Chemical Regent Co.) were dissolved in 1 L of ethylene glycol (99%, Beijing Chemical Reagent Co.) to form a 0.1 mol/L solution. Then 56 g of HCS powder was added into the solution. The mixed slurry was cooled to 0 °C, and 16.3 g of Zn powder (99.9%, 325 mesh, Beijing Chemical Regent Co.) with 100% stoichiometric amount for replacing Sn^{2+} and Sb^{3+} was added into the solution slowly and stirred simultaneously. The addition of Zn powder lasted 1.5 h. The product was washed by ethanol and filtered until Cl^- cannot detected by $AgNO_3$ solution. Finally, the product was dried under vacuum at 55 °C for 12 h. The obtained nano-SnSb/HCS composite was named CNSS. The weight percent of Sn, Sb, and Zn in the composite was 13.2%, 16.5%, and 1% in the samples according to chemical analysis. So, the weight percent of HCS is 70.3%. No Cl^- can be detected by EDS.

Electrochemical Tests. The electrochemical performances of the sample were investigated by using a Li/CNSS coin cell. The CNSS electrode film was prepared by coating slurries of the CNSS powders (95 w/o) with poly(vinylidene fluoride) as a binder dissolved in *N*-methylpyrrolidone on a copper foil. After drying and pressing under pressure of 1 MPa, the active mass in the electrode sheet was about 8 mg/cm^2 and 1.33 g/cm^3. (The thickness of the active mass layer was about 60 μm.) Li foil was used as the counter electrode, and the electrolyte was a solution of lithium hexafluorophosphate ($LiPF_6$) in a 50/50 vol % mixture of ethylene carbonate (EC) and diethyl carbonate (DEC) with concentration of 1 mol/L (Battery grade, Beijing Phylion Battery Co., Ltd.). The cell was assembled in an argon-filled glovebox (H_2O, <1 ppm, MBRUN, Labmaster. 130). It was cycled between 0 and 2 V under a constant current density of 0.2 mA/cm^2 by an automatic charger (Land BTI-10, China).

Characterization. X-ray powder diffraction was performed by using a Rigaku B/max-2400 X-ray diffractometer with Cu Kα radiation. A JEOL-2010 transmission electron microscope operating at 200 kV was used to observe the microstructure of the CNSS. The sample for HRTEM was prepared by standard mechanical thinning and ion milling. A Brunauer−Emmett−Teller (BET) measurement was conducted at 77 K on an absorptometer (MicromeritiHCS Instrument Corp. ASAP 2405N series) with a continuous adsorption procedure. Before measurement, sample was evacuated for 6 h at 523 K and 10^{-3} Torr.

(17) Wang, Q.; Li, H.; Chen, L. Q.; Huang, X. J. *Carbon* **2001**, *39*, 2211−2214.

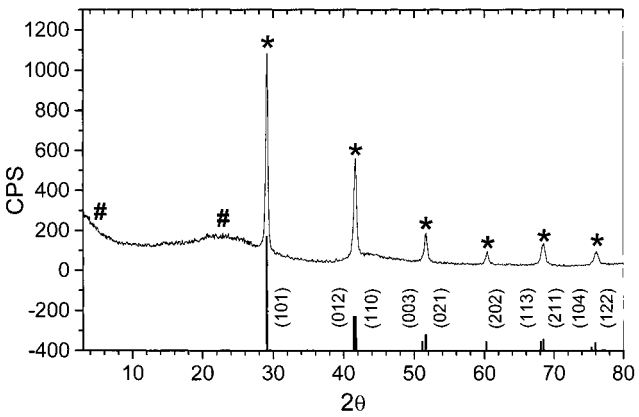

Figure 1. XRD pattern of a carbon/SnSb composite material (named CNSS). All peaks marked by * belong to β-SnSb; those marked by # correspond to non-graphitic carbon. The bottom column figure is drawn from the data in JCPDS 33-0118; λ = 1.5405 Å.

Figure 2. SEM image of the nongraphitic carbon: hard carbon spherules (named HCS).

The morphology of the electrode was observed by a Hitachi S-4000 scanning electron microscope. The procedures for investigating Li-inserted electrodes were similar to those in our previous report[15] and described briefly here. An electrode film after being discharged to 0.0 V and an electrode film after being discharged to 0.0 V and then recharged to 2.0 V were taken out from two Li/CNSS cells. After washing by anhydrous dimethylcarbonate (H_2O, <7 ppm, Beijing Phylion Battery Co.) to remove remnant electrolyte, the electrode films were dried in the vacuum chamber of the glovebox. Then, they were pasted directly onto a special shelf for SEM investigation in the glovebox and sealed in a glass bottle. During the transfer of the sample shelf from the sealed bottle into the vacuum chamber of the electron microscope, high pure argon gas flow was blown onto the surface of the shelf continuously to minimize the influence of moisture. The whole transfer process was finished within several seconds.

Results and Discussion

In the present work, a SnSb alloy was selected to pin onto a carbon surface because its crystal structure transforms from single-phase β-SnSb into multiple phases of Li_3Sb and Li_xSn (x < 4.4) during Li insertion; then the separated phases can be restored into the original β-SnSb phase after Li extraction.[13] This reversible structural variation is beneficial to the cyclic performance.

The XRD patterns of the as-prepared CNSS are shown in Figure 1. The non-graphitic structure of the

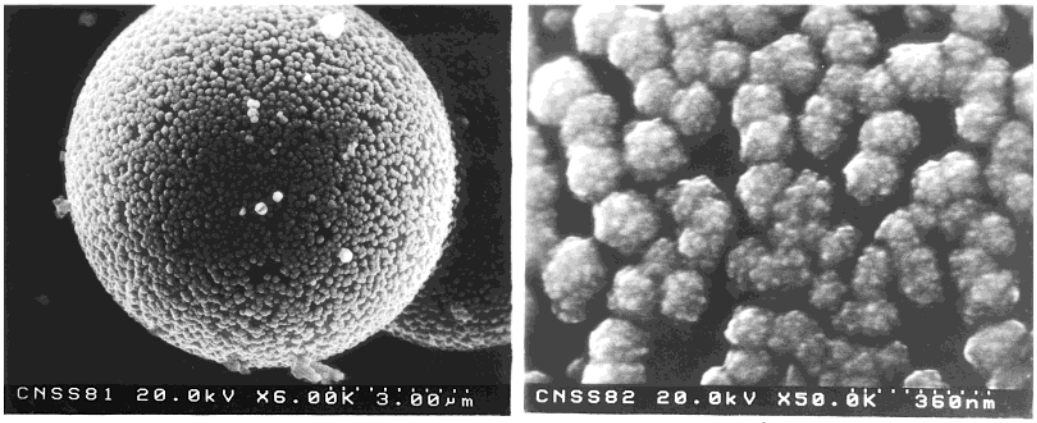

Figure 3. SEM images of the CNSS. Core carbon is the HCS: (a) low magnification; (b) local zoom of the surface region of a spherule.

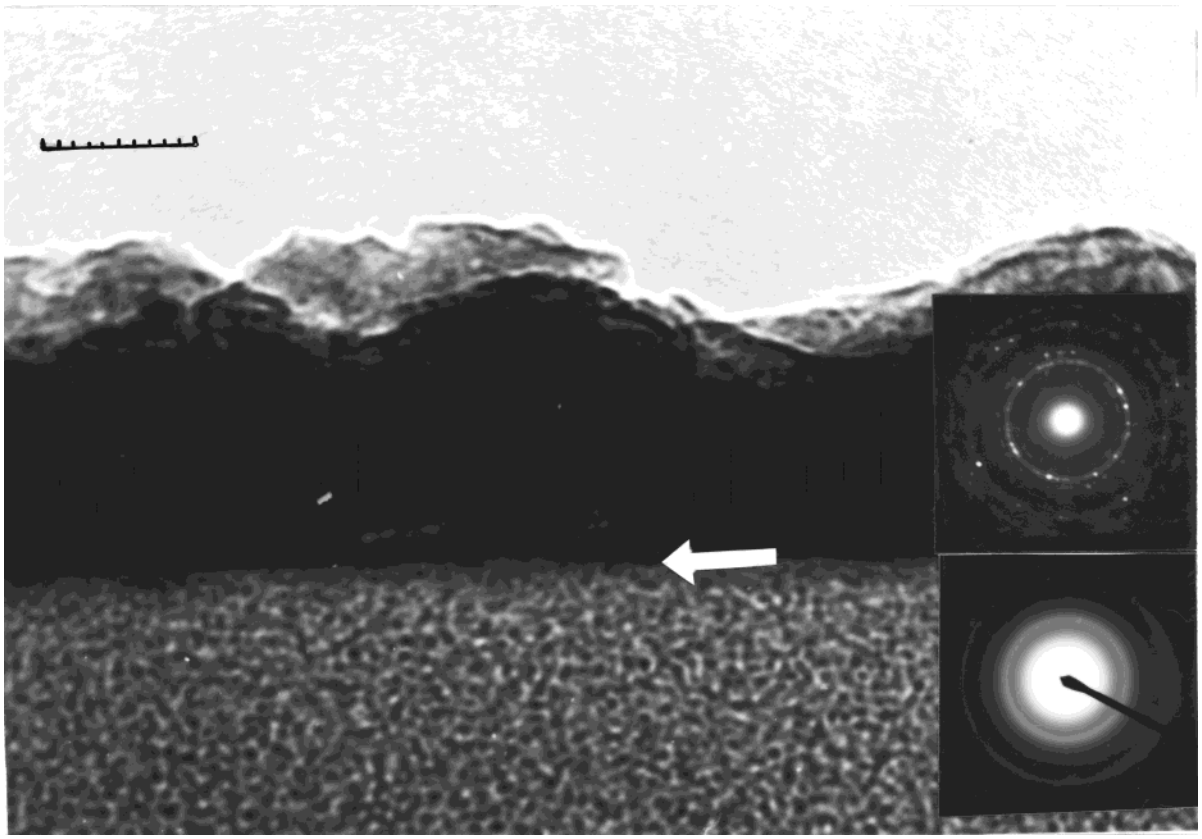

Figure 4. HRTEM image and SAED patterns of a CNSS particle. Inset: SAED patterns correspond to the edge region (up) and the core region (bottom) of the CNSS particle. The scale bar is 20 nm.

HCS is reflected by a broad peak at around 23°. The "tail" in the low Bragg angle region indicates a porous structure for the material. The peaks marked with an asterisk correspond to the rhombohedral phase β-SnSb (JCPDS, 33-0118). The grain size of β-SnSb is about 25 nm, as estimated from the Scherrer equation.

The morphology of the HCS is shown in Figure 2. The HCS has perfect spherical shape and smooth surface. Some particles have a peanut structure connected by a few spherules. According to the images of the CNSS in Figure 3, most of the SnSb alloy particles with an average diameter of 100 nm are dispersed on the surface of the HCS particles uniformly and separated, as expected. It can be also seen in Figure 3B that each alloy particle is composed of many small grains with a diameter of 20−30 nm, which is consistent with the XRD data.

The HRTEM image of a cross section of a CNSS particle is shown in Figure 4. The shallow core region is an amorphous structure, according to the SAED pattern in the bottom inset figure. It is composed of many micropores, less than 1 nm, which is also confirmed by the BET measurement.[17] The presence of micropores is also consistent with the XRD data in Figure 1. The edge region is nanosized SnSb alloy crystallites according to the SAED pattern in the top inset figure. Because of overlapping, the grains in each SnSb particles are not easy to be distinguished from the image. A key feature is that all of the alloy particles are connected to the carbon surface without observable

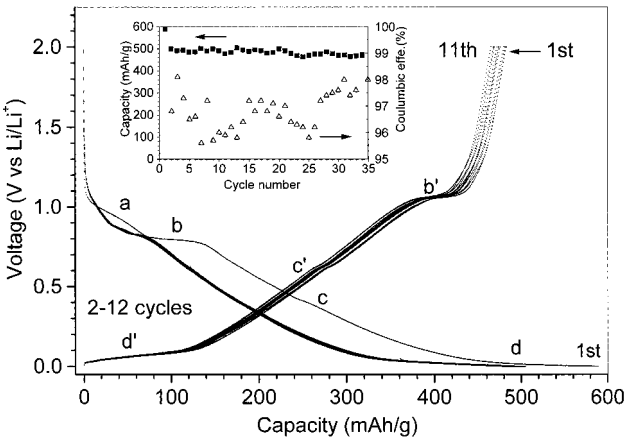

Figure 5. Discharge and charge curves of a CNSS electrode in a test cell CNSS/1 M $LiPF_6$, EC-DEC (1:1 in v/v)/Li. The letters marked in the figure represent different electrochemical reactions and explained in main text. The inset figure shows the relationship between Li insertion capacity and cycle number (solid square, left axis) as well as Coulombic efficiency at 2−35 cycle (hollow triangle, right axis).

cracks or cavities. In addition, the contrast of the boundary region shows a gradient variation from the outside to inner region of the carbon. This may imply that some alloy atoms penetrate into the micropores of the HCS. Therefore, it is believed that alloy particles are tightly pinned onto the carbon surface.

The Li storage behavior of CNSS was investigated by using a typical two-electrode Li/CNSS coin cell (Figure 5). The voltage profiles indicate different electrochemical reactions occurred on the CNSS electrode. During the Li insertion process, a slope (*a*) ranging from 1.1 to 0.8 V appears at the first discharge curve and disappears in the later cycles. This is mainly attributed to the decomposition reaction caused by a small amount of surface oxide on the nano-SnSb.[14] The plateau (*b*) at 0.8 V in the discharge curve and (*b*′) at 1.1 V in the charge curve is related to the alloy reaction of Li with Sb.[13] The multistep Li−Sn alloy reactions should be in the voltage region (*c*), ranging from 0.7 to 0.2 V.[1,6,13,14] Because of the small particle size of the alloy particles and the special crystal structure in which dual active elements coexisted in the alloy, the voltage profiles in the range (*c*) are very smooth, rather than having a multiplateau characteristic.[14] The insertion reaction of Li into the non-graphitic carbon also presents a slope ranging from 0.7 to 0.1 V in addition to a plateau from 0.1 to 0.0 V.[4,16] In addition, irreversible electrolyte decomposition reactions occur on the surface of the SnSb alloy and exposed HCS in the range 1.2−0.2 V.[13,14,17,18] Therefore, the curve in the region (*c*) was contribution from the three reactions as mentioned above, and the part in the region (*d*) is mainly related to the insertion of lithium into the micropores of HCS.

Compared with pure Sn, Sb, and the nano-SnSb alloy,[13,14] Li−Sb and Li−Sn alloying reactions on CNSS show much better cyclic performance. This may be related to the stable structure of the alloy in the CNSS. The images of the CNSS electrode at Li insertion state are shown in Figure 6A,B with different magnification. The images of the CNSS electrode at Li extraction state are shown in Figure 6C,D. For the alloy particles, there are two types of positions on the carbon surface. One is in the boundary regions where two HCS particles are in contact. Another is in the open area (without contact), which constitutes the majority of the HCS surface. In the Li insertion state, all alloy particles in the open area are separated while in the boundary region the alloy particles aggregate with each other leading to the connection of two or more the CNSS particles (see Figure 6A,B). In the Li extraction state, SnSb alloy particles in the open area are still separated, but the connected composite particles are not separated (see Figure 6C,D). Obviously, the goal of hindering electrochemical agglomeration of the alloy particles has been achieved in the open area completely. On the other hand, the size of the agglomerates in the boundary regions could not develop too greatly due to the low amount of free alloy particles. In addition, nanosized SnSb alloy particles either in the open area or in the boundary regions are still pinned on the HCS surface tightly after Li insertion and extraction (Figure 6A,C). Consequently, the cyclic performance of the CNSS is promising.

In addition, the original micropore volume of HCS is 0.18 mL/g, and that of CNSS is 0.071 mL/g according to BET measurements. This may be caused by the covering or filling of some alloy clusters into the micropores near the surface regions of the HCS particles. In any case, those alloy clusters may act as the "root" for outer larger alloy particles as mentioned before. It is beneficial to enhance the stability of the nanoalloy particles on the surface of the HCS particles, especially during electrochemical cycling.

All elements in the composite materials are active for Li storage and contribute to the reversible capacity for the CNSS. The measured value is 480 mA h/g, close to the calculated value, 489 mA h/g, and a little lower than the theoretical value, 548 mA h/g. (The theoretical capacity of SnSb is 824 mA h/g; the practical capacity for the HCS and the SnSb alloy cycled in the voltage range of 0−2.0 V is 430[16] and 629 mA h/g,[13] respectively.) This value is much higher than that of graphitic carbon (<372 mA h/g). Moreover, the pinning layer of 29.8% SnSb alloy only increases the volume for each HCS particle by 4−5% since the particle size of the alloy is around 100 nm. Therefore, the CNSS shows a 16% increase in the volumetric capacity compared with the HCS itself. However, the reversible volumetric capacity of the CNSS is only about 640 mA h/cm^3 due to low tap density of the HCS (0.8 g/cm^3, its true density = 2.0 g/cm^3). It is lower than that of graphitic carbon anodes in Li ion batteries (800 mA h/cm^3). Therefore, the CNSS in this case may be used in the batteries needing high gravimetric capacity. Furthermore, it has been confirmed that both the gravimetric and volumetric capacity can be adjusted by different combination of carbon and alloys.[18,19]

The Coulombic efficiency for CNSS at the first cycle is 82% as evaluated from Figure 5. It is much higher than the estimated value 70%. (The Coulombic efficiency and discharge capacity of the nano-SnSb and the HCS

(18) Shi, L. H.; Li, H.; Chen. L. Q.; Huang, X. J. *J. Mater. Chem.* **2001**, *11*, 1502−1505.

(19) Shi, L. H.; Li, H.; Wang, Z. X.; Chen, L. Q.; Huang, X. J. Submitted to *Solid State Ionics*.

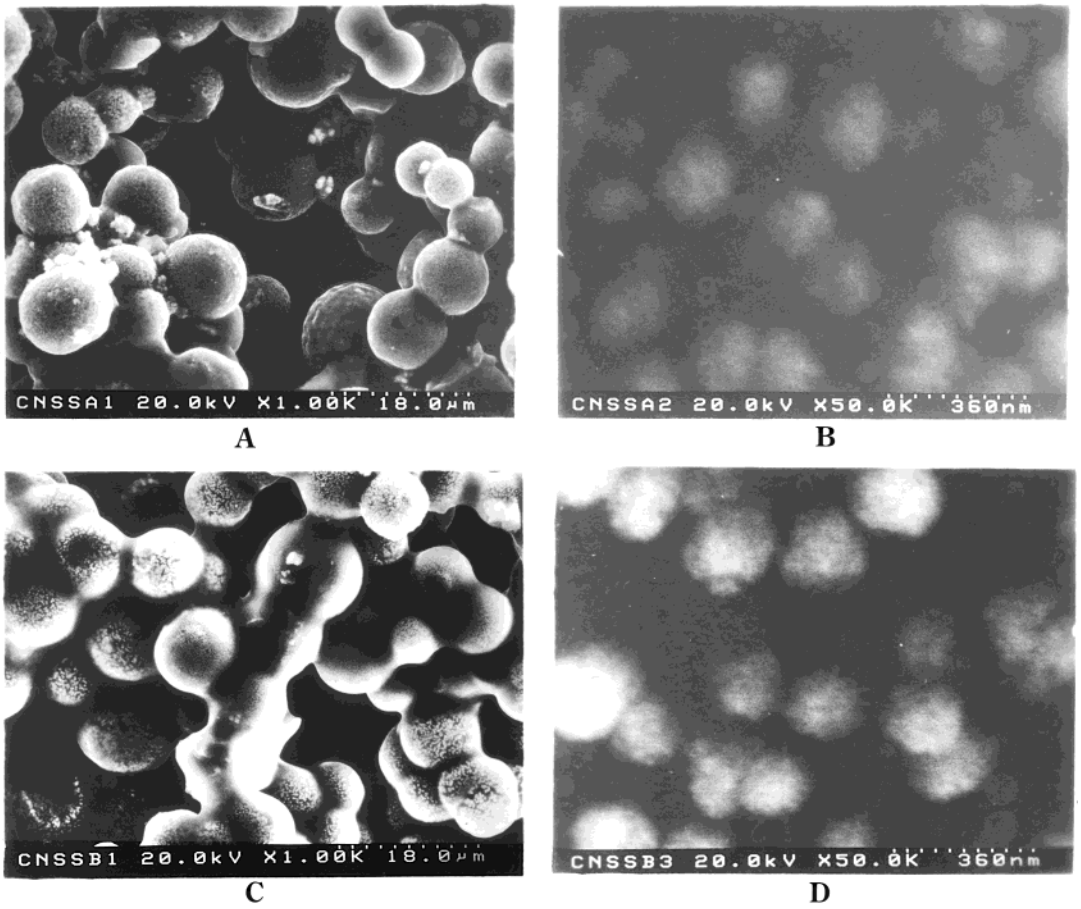

Figure 6. SEM images of the CNSS electrodes: (A) Li insertion state, the corresponding cell was discharged to 0.0 V; (B) the same electrode as (A), but at higher magnification; (C) Li extraction state, the corresponding cell was discharged to 0.0 V and then charged to 2.0 V at a current density of 0.2 mA/cm^2; (D) the same electrode as (C), at higher magnification.

samples at the first cycle in test batteries = 63%/704 mA h/g and 73.8%/567 mA h/g, respectively.[11,13,17]) The irreversible capacity loss for pure phase nano-SnSb is mainly related to the formation of a solid electrolyte interphase (SEI) layer and the decomposition of the surface oxide, which is proportional to the surface area of alloy exposed to the electrolyte.[13,14] For non-graphitic carbon treated at 1000 °C, the capacity loss is also mainly caused by the formation of the SEI.[20−22] It is expected that the surface area of both alloy and carbon exposed to the electrolyte will decrease if the alloy particles are tightly pinned onto the surface of the carbon. In fact, the measured BET area of the CNSS is around 159 m^2/g from the nitrogen adsorption−desorption isotherm while the original BET area of the HCS is 400 m^2/g.[17] This may explain the improvement of the Coulombic efficiency at the first cycle.

However, it is noticed that the Coulombic efficiencies at following cycles are not as high as 100% as shown in the inset figure in Figure 5. It fluctuated from 96% to 98%. This implies a capacity loss in each cycle. It may be related to unstable SEI film on the nanoalloy surface and the irreversible trapping of Li ions by the alloy/carbon composite.[14] In test lithium cell, loss lithium at each cycle can be compensated by excess lithium from the counter electrode metal Li foil, while it will lead to rather poor cyclic performance in practical Li ion batteries. This problem seems difficult to be solved completely only by pinning mode.

On the basis of above results and discussion, it seems that preventing nanoscale alloy particles from contacting with the electrolyte solution is very necessary for avoiding the formation of unstable SEI film on the alloy particles, which is one of the main reasons leading to low Coulombic efficiency in the first cycle and the following cycles of the CNSS. A possible method is to prepare an alloy/carbon composite, in which all of the alloy clusters or nanocrystallites occupy the micropores and mesopores of the carbon so that the formation of unstable SEI film on alloy particles, pulverization, and agglomeration of alloy particles can be prevented completely. In addition, the volumetric capacity can be also increased. Further work is underway to test this assumption.

Conclusions

Pinning nanosized alloy particles tightly onto the carbon surface enhances the dimensional stability of the alloy particles during Li insertion and extraction. Consequently, the composite material shows much better cyclic performance. In addition, its Coulombic efficiency at the first cycle is 82%, much higher than the estimated value 70% from that of two precursors.

(20) Mabuchi, A.; Tokumitsu, K.; Fujimoto, H.; Kasuh, T. *J. Electrochem. Soc.* **1995**, *142*, 1041−1046.
(21) Matsumura, Y.; Wang, S.; Mondori, J. *J. Electrochem. Soc.* **1995**, *142*, 2914−2918.
(22) Xing, W.; Dahn, J. R. *J. Electrochem. Soc.* **1997**, *144*, 1195−1201.

The improvement may be related to the decrease of the surface area exposed to the electrolyte. The gravimetric capacity of the composite is as high as 480 mA h/g. However, it shows low volumetric capacity of 640 mA h/cm^3 and rather low Coulombic efficiency at following cycles. The latter may be caused by the formation of an unstable SEI film on the nanoalloy surface and irreversible trapping of Li ions by the alloy/carbon composite. Despite these drawbacks, the combination of the alloy and the carbon in a designed structure show great potential for improving the energy density of Li ion batteries.

Acknowledgment. This work was supported by NSFC (No.59972041) and the National 863 key program.

CM010195P